Electronic and vibrational radiative cooling of the small carbon clusters C_4^- and C_6^-

N. Kono,* R. Suzuki, T. Furukawa,† J. Matsumoto, H. Tanuma, and H. Shiromaru
Faculty of Science, Tokyo Metropolitan University, Hachioji, Tokyo, 192-0397, Japan

T. Azuma
Atomic, Molecular and Optical Physics Laboratory, RIKEN, Wako, Saitama, 351-0198, Japan

K. Hansen
Joint Center of Quantum Studies and Department of Physics, Tianjin University, Tianjin 300072, China
and Department of Physics, Gothenburg University, 41296 Gothenburg, Sweden

(Received 4 October 2018; published 28 December 2018)

Delayed electron detachment yields of C_4^- and C_6^- induced by photoexcitation in an electrostatic ion storage ring were measured as functions of excitation energies and laser firing times, allowing for a mapping of their radiative cooling in a wide energy range. The energy window concept and discrimination of one- and two-photon absorption are critical in understanding the obtained results. The experimentally obtained electronic and vibrational cooling rates were consistent with a simulation based on detailed-balance theory. The even-odd alternation of vibrational cooling rates, predicted from IR intensities, was also examined. We found that the larger anion cools faster, with no indication of an even-odd alternation.

DOI: 10.1103/PhysRevA.98.063434

I. INTRODUCTION

The understanding of radiative cooling of hot molecules has been drastically improved by the recent development of ion storage devices such as storage rings and ion traps [1]. In the highly isolated environment realized in such devices, the internal conversion (IC) process by which the electronic energy is distributed to various vibrational modes is no longer irreversible. That is, an inverse internal conversion (IIC) process will occur, and the energies distributed into various vibrational modes may revert to electronic energy with a certain probability.

In general, radiative cooling has been considered purely vibrational. For example, the cooling of hot C_5^- and C_7^- stored in a ring can be explained solely by the vibrational radiative cooling [2,3].

However, sometimes IIC is not negligible. For example, cooling rates of fullerene anions [4], polycyclic aromatic hydrocarbons (PAHs) ($C_{14}H_{10}^+$ [5] and $C_{10}H_8^+$ [6]), semiconductors (B_8^+ – B_{18}^+ [7] and Si_5^+ – Si_{13}^+ [8]), metal clusters (Al_4^- and Al_5^- [9]), and small carbon clusters (C_6^- [10,11] and C_4^- [12]) are found to be much higher than expected for vibrational radiative cooling alone. The electronic radiative cooling process referred to as recurrent fluorescence (RF) cooling, with its visible or near infrared (NIR) photon emission via the electronic excited states regenerated through IIC, is invoked to explain this discrepancy. For very large molecules and particulate matter, the emission of visible photons from hot species is not surprising; it is a well-known consequence of black-body radiation. However, fullerenes are definitely not described as particulate matter, and the other clusters examined are even smaller. For instance, RF photons were directly detected from C_6^- [13] and C_4^- [14].

The fact that RF cooling is found only for the even-numbered carbon cluster anions is a manifestation of the even-odd alternation generally found for chain-forming carbon clusters. That is, these anions show an even-odd alternation in the electronic structures; only even-numbered cluster anions posses low-lying electronic excited states, which is required for the RF process. In summary, the cooling scheme of the carbon cluster anions is as follows:

(1) (n: odd)

$$C_n^{-*(e)} \rightarrow C_n^{-*(v)} \rightarrow C_n^- + \text{IR photons}$$

(2) (n: even)

$$C_n^{-*(e)} \rightarrow C_n^{-*(v)} \rightarrow C_n^- + \text{IR photons}$$

$$C_n^{-*(e)} \rightarrow C_n^{-*(v)} \rightarrow C_n^{-*(e)} \rightarrow C_n^- + \text{vis or NIR photons},$$

where $C_n^{-*(e)}$ and $C_n^{-*(v)}$ are anions in their electronic and vibrational excited states, respectively, above the electron detachment threshold.

The electronic excited states of C_4^- and C_6^- are shown in Table I. Low-lying, optically active electronic excited states are present in each anion. The C-X transitions are favored by their very large cross-sections [16]. The B-X (C_4^-) and A-X (C_6^-) transitions are instead favored by high populations of the B (C_4^-) and A (C_6^-) states due to their lower energies, which allows the RF to happen also at lower excitation energies for these anions. The energy regions surveyed so far, as shown in Table I, are mostly above the lowest electronic excited states, with RF processes having been observed from these states.

Previously, the RF rates in the vicinity of the electron detachment thresholds E_{th} of C_4^- and C_6^- (electron affinity

*Corresponding author: kouno-naoko@ed.tmu.ac.jp
†Present Address: Department of Physics, Toho University; takeshi.furukawa@sci.toho-u.ac.jp

 ©2018 American Physical Society

TABLE I. Excitation energies of the electronic states of C_4^- and C_6^- [15–19] and the internal energies of anions where electronic or vibrational cooling rates were measured previously [10–12,20]. The rightmost column shows the energies studied in this work. The A state of C_4^- and the B state of C_6^- are dipole-forbidden with respect to their corresponding X state. All energies are given in eV.

	State	Reported	This work
C_4	$X\ ^3\Sigma_g^-$ 3.88	3.88	
	$C\ ^2\Pi_u$ 2.71		
		1.88, 1.97, 2.06, 2.08	
		1.40, 1.54, 1.55, 1.74	
	$B\ ^2\Sigma_u^+$ 1.34		
	($A\ ^2\Sigma_g^+$ 1.00)	1.30	1.06
C_4^-	$X\ ^2\Pi_g$ 0.00		0.62, 0.92
C_6	$X\ ^3\Sigma_g^-$ 4.18	4.18, 4.45, 4.49	
	$D\ ^2\Pi_g$ 2.49		
	$C\ ^2\Pi_g$ 2.04		2.15, 2.24, 2.28
	($B\ ^2\Sigma_u^+$ 1.32)		1.91, 2.01
	$A\ ^2\Sigma_g^+$ 1.16		
C_6^-	$X\ ^2\Pi_u$ 0.00	0.36	0.34, 0.40, 0.53

of neutrals) were determined by analyzing the measured decay of neutral yields after laser excitation [10–12,20]. In addition, the energies just above the B state of C_4^- were monitored by recording the neutral yields as a function of time between ion generation and laser excitation ($\simeq$ laser firing time or ion storage time, t_{las}). The RF cooling rate below the detachment threshold was obtained from the energy window concept, which will be explained below.

The fact that RF cooling is observed only for the even-numbered hot cluster anions leads to the question of whether the *vibrational* radiative cooling also shows an even-odd alternation. Assuming that the structures of the hot anions are linear, the vibrational cooling of these carbon clusters mainly proceeds through a single mode of antisymmetric stretching, with significantly stronger IR intensity than the others (see Table II). In short, the expected propensity is that the even-numbered anions cool slower. It should be noted that we chose the results found in Ref. [21] instead of those found in Ref. [22] to compare to our results because the first reference gives the series of measured clusters calculated with the same method. A comparison of different sizes with this choice will therefore avoid assigning physical differences to different methods of calculation.

TABLE II. Vibrational quantum energies (cm^{-1}) and IR intensities (km mol^{-1}) of the relevant modes for C_n^- ($n = 4 - 7$) [2,21].

Ion	Vibrational quantum energy	IR intensity	Mode
C_4^-	1785	87	ν_3 (σ_u)
C_5^-	1807	855	ν_3 (σ_u)
C_6^-	2037	726	ν_4 (σ_u)
C_7^-	1836	2331	ν_5 (σ_u)

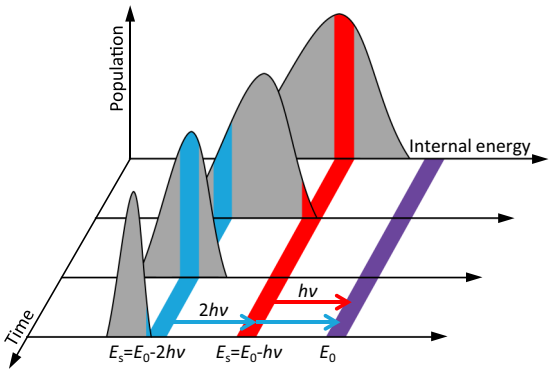

FIG. 1. Schematics of the time evolution of the sampled population during the cooling process, where E_0 is the energy window, $h\nu$ is the photon energy of the laser, and $E_s = E_0 - h\nu$ and $E_s = E_0 - 2h\nu$ are the sampled energy for one- and two-photon absorption, respectively. Multiphoton absorption may be observed depending on the photon energy and time after ion generation.

The radiative cooling of small anions with internal energies below the detachment threshold was mainly studied by employing the energy window concept. Here the yields of delayed detachment induced by laser irradiation were measured as a function of t_{las} at a fixed laser wavelength. The procedure providing information on the time evolution of the energy distribution from the t_{las} dependence is shown schematically in Fig. 1, illustrating the window concept. This works because, for small anions, the rate of delayed detachment is a rapidly increasing function of internal energy. Thus, the laser-induced neutrals detected in a specific delay after the laser pulse will come from anions with a specific internal energy, called the "energy window (E_0)", as indicated by the purple area in Fig. 1. The observed yield is proportional to the population of ions at E_0 and therefore to the population at the sampled energy $E_s = E_0 - nh\nu$ just prior to photon absorption. For the observation of the decay yield at a specific time after laser excitation, the internal energy of the decaying species is fixed. When the photon energy is constant, the cross sections of the absorbing species are also constant, and in particular, independent of the ion storage time preceding the laser pulse. The neutral yield is therefore rigorously proportional to the prelaser population of the ion at the specific excitation energy probed. Based on this concept, multiphoton processes lead to the sampling of populations at lower internal energy.

Utilizing this window concept, RF cooling of C_4^- [12] as well as the vibrational cooling of C_5^- [2], C_7^- [3], and C_6H^- [10] were studied. Very recently, precise values of the RF and vibrational cooling rates of C_6^- were obtained by an electrostatic ion beam trap study [20].

In this paper, the RF and vibrational radiative cooling of C_4^- and C_6^- in a wide internal energy range, 0.43–2.24 eV for C_4^- and 0.34–2.28 eV for C_6^-, will be presented. For C_4^-, only vibrational cooling was studied; the RF rate of C_4^- has been reported in our previous study [12]. For C_6^-, the RF and vibrational cooling rates were obtained and compared to the previously reported values [20]. The even-odd alternation in vibrational cooling will also be discussed in light of the results of C_5^- and C_7^- reported previously [2,3].

II. EXPERIMENTS AND SIMULATION

The experiments were performed at the electrostatic ion storage ring "TMU E-ring" [23] with a laser-ion beam merging configuration shown schematically in Fig. 2.

Hot carbon cluster anions produced in a laser ablation ion source were stored in the ring at a kinetic energy of 15 keV. At a certain laser firing time, up to 90 ms after ion generation, the ions were reheated by photons from an optical parametric oscillator (OPO) (Spectra-Physics MOPO-SL) pumped by a pulsed Nd: YAG laser (Spectra-Physics Quanta-Ray Pro-230-10) at the straight section on the side opposite to that of neutral detection. The neutral particles, which appeared due to delayed electron detachment, were detected by a set of microchannel plates (MCPs) half turn after the photon absorption. The detection of neutrals occurs more than 10 μs after laser excitation due to the circulation periods of C_4^- and C_6^- (about 32 and 39 μs, respectively). The laser pulse energy was kept below 3 mJ/pulse with a pulse duration below 10 ns. Under these irradiation conditions multiphoton absorption may still occur; thus, the neutrals induced by one- or two-photon absorption were detected.

The procedure used in the simulation of RF and vibrational radiative cooling was basically the same as that reported previously [12,24]. In brief, a detailed-balance theory was used to calculate the energy-dependent detachment rate, which was then used to determine the detectable portion of generated neutrals and hence the energy window. Rotational cooling was ignored because it is much less effective than other decay channels [25]. The level densities were calculated assuming that all the vibrations are harmonic. The theoretical value of the RF rate $k^i_{\rm RF}(E)$ is given by

$$k^i_{\rm RF}(E) = f_{\rm RF} A^i_{\rm RF}\, g_i(E), \quad g_i(E) = \frac{\rho\left(E - E^i_{\rm RF}\right)}{\rho(E)}, \qquad (1)$$

and that of the vibrational cooling rate $k^j_{\rm v}$ is given by

$$k^j_{\rm v}(E) = f_{\rm v} A^j_{1-0} \frac{1}{\rho(E)} \sum_n n\rho_j(E - nh\nu_j). \qquad (2)$$

The definitions of the terms are as follows: $A^i_{\rm RF}$ is the A coefficient for the electronic transition from the ith excited state to the ground state, $g_i(E)$ is the population of the i-th electronic state for the total internal energy E, $\rho(E)$ is the level density taking into account all the vibrational modes, $E^i_{\rm RF}$ is the energy of the ith electronic excited state, A^j_{1-0} is the A coefficient for vibrational transition, ρ_j is the level density without the jth vibrational mode, and n is the vibrational quantum number. $f_{\rm RF}$ and $f_{\rm v}$ are scaling factors on the order of unity. They are introduced to match the experiment and theory by compensating for any idealization in the description. The vibrational energy emission rate $P_{\rm v}(E)$ is therefore given by

$$P_{\rm v}(E) = \sum_j h\nu_j k^j_{\rm v}(E), \qquad (3)$$

where $h\nu_j$ is the emitted photon energy for the jth vibrational mode.

The RF cooling rates $k_{\rm RF}(E)$ were obtained directly by fitting the $t_{\rm las}$ dependence without the need of simulations. On the other hand, the vibrational cooling rates $P_{\rm v}(E)$ were obtained by comparing the experimental and simulated $t_{\rm las}$ dependence curves. For this purpose, neutral yields were calculated for the simulated energy distribution as a function of $t_{\rm las}$, and the scaling factor matched to reproduce the experimental yield curves. The time variation of the population at the sampled energy $E_{\rm s}$ was calculated as follows: the initial internal energy distribution was assumed to be of Boltzmann type with an effective temperatures of 5000 K at the time of ion generation, i.e., the Boltzmann factor multiplied by the vibrational level density. Then the time evolution of the distribution was calculated, considering the depletion by electron detachment (loss of ions) and energy loss due to electronic and vibrational cooling.

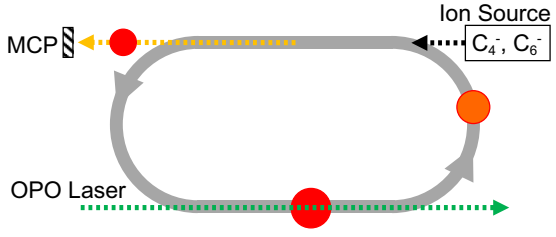

FIG. 2. Experimental scheme of TMU E-ring [23].

III. RESULTS AND DISCUSSION

A. Radiative cooling of C_6^-

The energy window E_0 is located at 4.49 eV for C_6^-, slightly above $E_{\rm th}$ (4.18 eV), and has a width of 0.16 eV. Typical $t_{\rm las}$ dependence plots of the neutral yields for C_6^-, obtained with 550 and 480 nm laser irradiation, are shown in Figs. 3(a) and 3(b), respectively. The plots show the evolution of the population $g(E_{\rm s})$ at the sampled energy $E_{\rm s}$. The yield curves are observed to behave differently in earlier (I) and later (II) time regions. At the earlier time region I, the yields quickly decrease, both in Fig. 3(a) and 3(b). This is a typical feature of RF cooling, which removes so much energy that the upper-energy component of the energy distribution jumps into $E \ll E_{\rm s}$. Since $E_{\rm s}$ must be above the RF-active electronic states, the yields in this region are consequently due to one-photon ($E_{\rm s} = E_0 - h\nu$) processes. As for region II, an increase in the yield is seen in Fig. 3(a), indicating that the sampled energy is initially below the peak of the distribution. That is, the main contribution switches from a one-photon to two-photon ($E_{\rm s} = E_0 - 2h\nu$) process at around 10 ms when the high energy population $g(E_{\rm s} = E_0 - h\nu)$ is exhausted by the RF radiation. On the other hand, the yields do not increase in region II of Fig. 3(b). This is simply due to the negative value of $E_{\rm s} = E_0 - 2h\nu$ for 480 nm photons. In other words, two-photon excitation raises the energy of C_6^- to considerably above E_0 irrespective of its initial internal energy, and the resulting rate of detachment is too fast to be observed in the present experimental configuration. It should be noted that $E_0 - 3h\nu$ is negative for all laser wavelengths employed in this work.

Semilog plots of the fast decay components are shown in Fig. 4, obtained by (a) 480, (b) 500, (c) 530, (d) 550, and (e)

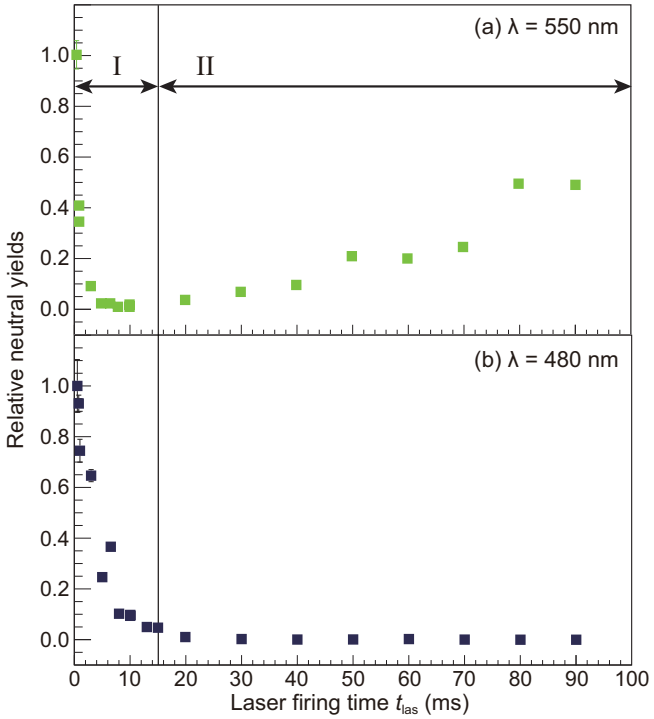

FIG. 3. Relative neutral yields of C_6^- as a function of laser firing time at wavelengths (a) 550 and (b) 480 nm.

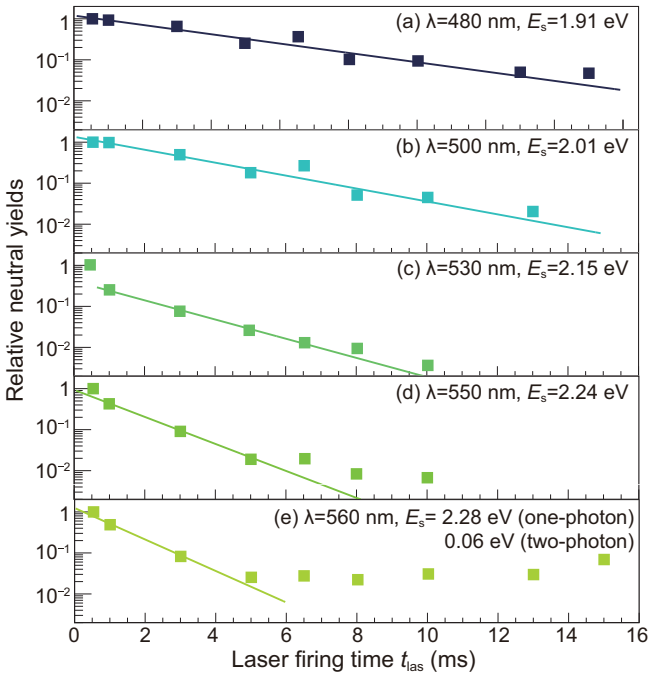

FIG. 4. Relative neutral yields of C_6^- as a function of laser firing time of up to 15 ms at wavelengths (a) 480, (b) 500, (c) 530, (d) 550, and (e) 560 nm. The plots in (a) and (d) are essentially the same data as those in region I in Fig. 3.

560 nm photons. The E_s values are shown in the figures. The yields decrease exponentially as expected and similar to the case of C_4^- in our previous study [12]. The slopes of the fast components, which give the RF rate constants at $E_s = E_0 - h\nu$, are steeper for longer wavelengths. As mentioned before, the RF cooling rates are directly obtained from these slopes. In Fig. 4(d), and more prominently in Fig. 4(e), slowly varying components due to two-photon processes appear. Thus, the E_s at $\lambda = 560$ nm consists of $E_0 - h\nu = 2.28$ eV and $E_0 - 2h\nu = 0.06$ eV. In Figs. 4(a) to 4(c), such components are also expected to be present but are hidden by the dominant one-photon process.

The experimental RF cooling rates for C_6^- are shown in Fig. 5 as a function of internal energy, together with those at higher energies reported previously [10,11]. The theoretical curve with the scaling factor $f_{RF} = 1.0$ (red line in Fig. 5) agrees well with the experimental plots except for a small vertical shift, as also seen for C_4^- in our previous study [12]. The curve reproduces the experiments even better in the wide range of the internal energies when the scaling factor f_{RF} is 1.8 ± 0.4, which agrees with the previous report [20] (black line in Fig. 5). The obtained RF cooling rates are adopted for the subsequent analysis of vibrational cooling behavior. Although the fast RF cooling is completed in the time range of vibrational cooling analysis, it should be taken into account because it determines the "initial" distribution that undergoes vibrational cooling.

The plots of neutral yields against t_{las} on a longer time scale up to 90 ms are shown in Fig. 6 for the longer wavelengths from 610 to 640 nm. The sampled energies $E_s = E_0 - 2h\nu$ are 0.34 eV (610 nm), 0.40 eV (620 nm), and 0.53 eV (640 nm). As shown in each plot, the yield initially increases (except the point at $t_{las} \simeq 0$) and at a specific laser firing time it starts decreasing due to cooling-induced depletion of the population in the upper energy region. The peaking time depends on E_s, with later times for lower values of E_s; i.e., higher photon energy, as expected. Such a peaking profile was also observed for the one-photon studies of C_5^- and C_7^- [2,3], and is consistent with the window concept.

From these simulated energy distributions, the time evolution of the population at E_s was obtained. When the scaling factor of the theoretical vibrational cooling rate (f_v) is 1.0, the theoretical neutral yield curves (red lines) do not reproduce

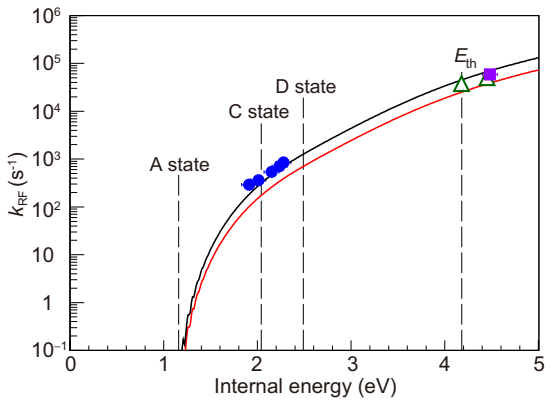

FIG. 5. Plots of the theoretical and experimental RF cooling rates of C_6^-. Lines are theoretical rates with $f_{RF} = 1.0$ (red) and $f_{RF} = 1.8$ (black), blue circles represent the result in this work, the purple square at 4.49 eV (E_0) is from our previous report [10], green open triangles at 4.18 eV (E_{th}) and 4.45 eV are the experimental values obtained by Chandrasekaran *et al.* [11].

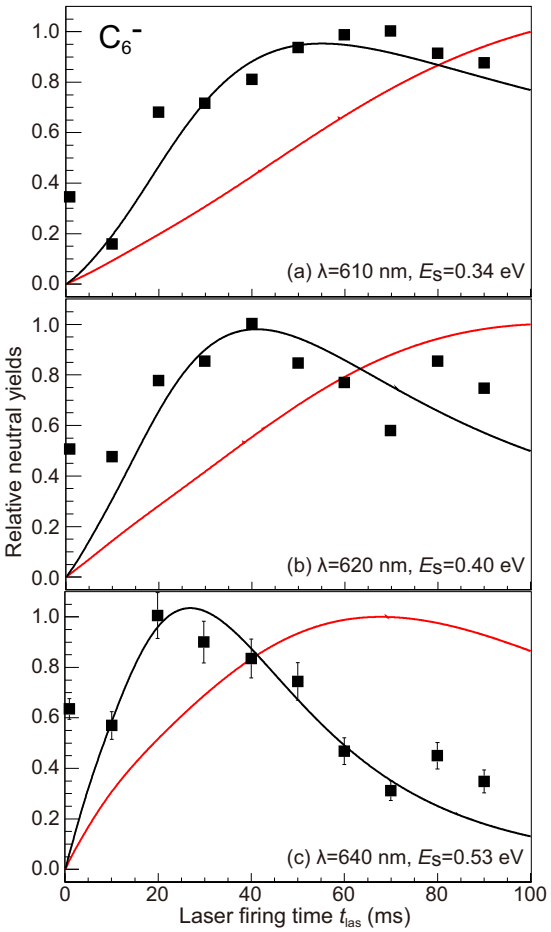

FIG. 6. t_{las} dependence of the relative neutral yields for C_6^- up to 90 ms at the wavelengths (a) 610, (b) 620, and (c) 640 nm. The yields are normalized to the peak value. The red lines are the simulated yield from the theoretical rates and black lines are those scaled by the factors of 1.8 for electronic and of 2.7 for vibrational cooling rates. The error bars are statistical. The points at $t_{las} \simeq 0$ in each plot are due to one-photon processes and are not included in the fitting.

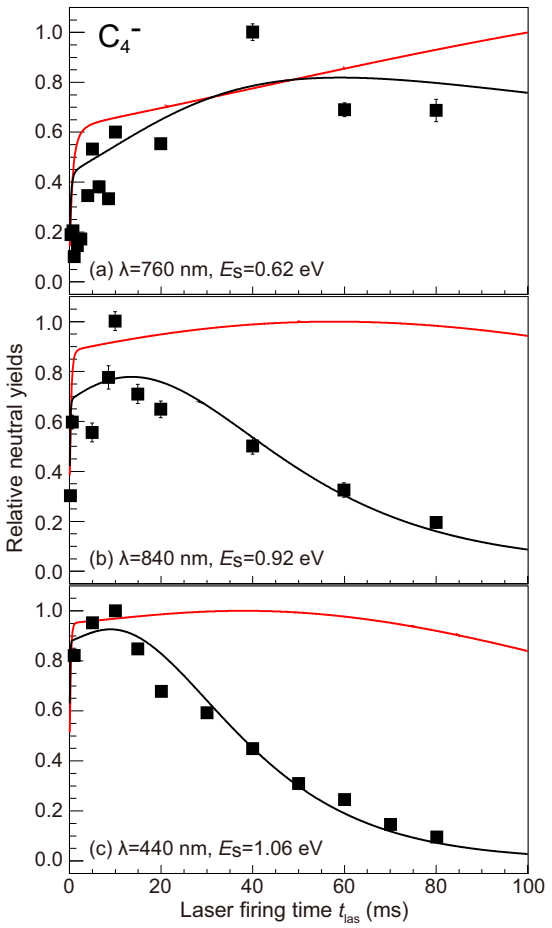

FIG. 7. t_{las} dependence of the relative neutral yields for C_4^- up to 80 ms at three different E_s. The wavelengths and E_s are shown in the figure. The red lines are the simulated yields from the theoretical rates and the black lines are those scaled by the factors of 2.7 for electronic and of 4.4 for vibrational cooling rates. The error bars are statistical. The points at $t_{las} < 5$ ms in each plot are due to the RF processes and are not included in the fitting.

the experiments, but instead indicates faster cooling than predicted. A scaling factor $f_v = 2.7 \pm 0.3$, which reproduces the time dependence of the yields for all wavelengths, was obtained by the fitting, as shown by the black lines in Fig. 6. This also agrees well with the reported value of the factor obtained previously by 606.9 nm two-photon absorption [20]. The experimentally scaled theoretical cooling rates obtained by this method will be discussed below.

B. Radiative cooling of C_4^-

As mentioned before, the RF cooling rates of C_4^- were measured previously using the energy window $E_0 = 3.88$ eV, which is approximately equal to the electron detachment threshold (3.88 eV) with a width of less than 1 meV [12]. The small width is due to the small heat capacity of C_4^-. The fitting of the experimental and theoretical values gives the scaling factor $f_{RF} = 2.7 \pm 1.2$ (see Fig. 7 in Ref. [12]). It should be noted that the RF rate constants at these energies are much larger than for C_6^-.

The t_{las} dependencies of the neutral yields up to 80 ms, induced by irradiation of 440 nm ($h\nu = 2.82$ eV), 760 nm (1.63 eV), and 840 nm (1.48 eV) photons are shown in Fig. 7. On this timescale, the decrease of the neutral yields induced by one-photon absorption of 760 and 840 nm light is too fast to be seen (faster than 5 ms) since it measures the population of highly excited states. In addition, two-photon absorption of 440-nm light, and three-photon absorption of 760- and 840-nm light elevates anions from the ground state to too far above E_0 to be detected in the present experiments. Thus the plots show the population changes at $E_s = 0.62$ eV (760 nm two-photon), 0.92 eV (840 nm two-photon), and 1.06 eV (440 nm one-photon) exclusively.

The vibrational cooling rates, or the scaling factors for the theoretical rate, are derived with the same procedure as employed for C_6^-. As in the case of C_6^-, simulations with $f_{RF} = 1.0$ (red lines in Fig. 7) show much slower decay than the experimental results. A scaling factor of $f_v = 4.4 \pm 0.3$ (black lines) gives a reasonable fit except at the very beginning of the storage. As for the short storage time region,

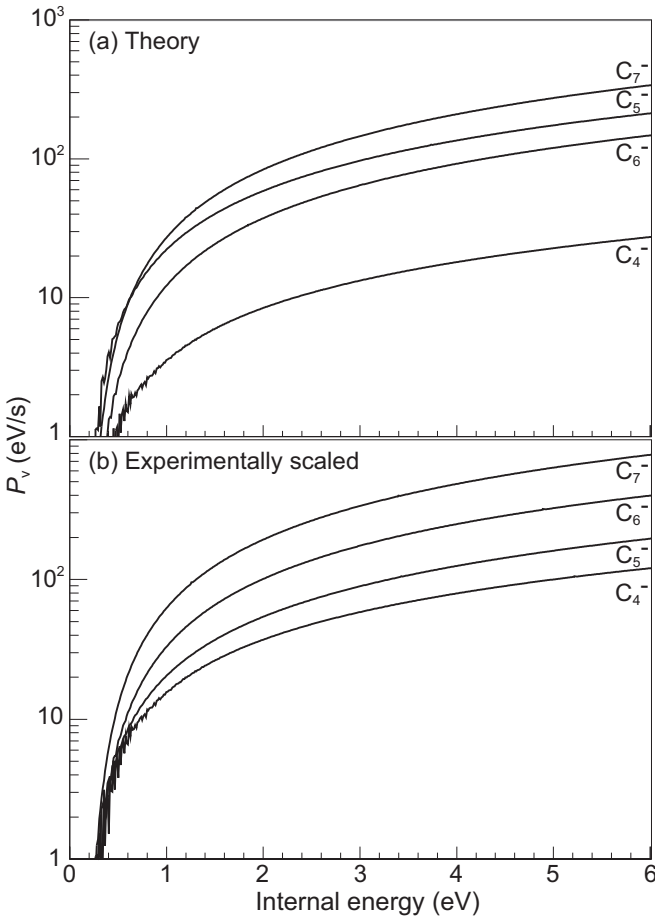

FIG. 8. Plots of the theoretical vibrational cooling rates (a) without any scaling of the emission rates and (b) experimentally scaled, against the internal energies for C_4^-, C_5^- [2,26], C_6^-, and C_7^- [3].

the simulations show much faster rise, and the lowering of the RF scaling factors does not improve the situation. Such disagreement is not observed for C_6^- (Fig. 6), probably due to the relatively small RF cooling rate. For C_4^-, the much faster RF rate strongly enhances incoming components from the region just below $E_{\rm th}$, leading to a sudden increase of the population at $E_{\rm s} = E_0 - 2h\nu$. It should be noted that the rise becomes slower if the broad feature of the emitted RF energies is taken into account. In fact, a recent RF photon detection study indicates that the RF emission is very broad [14]. The broad spectrum of the RF photon energy does not affect the RF cooling rate obtained from the rapid decrease of the population at the upper levels. It only has an influence on the increase of the population at the lower levels, the destination of the RF processes. Although further analysis must wait until the spectral features are determined in more detail, we conclude that the precise details do not affect the observed vibrational cooling rate.

C. Size dependence of vibrational cooling of C_n^-

To investigate the expected even-odd alternation in vibrational cooling rates, the theoretical cooling rates without scaling factors are shown in Fig. 8(a) for C_n^- ($n = 4$–7). Because of the aforementioned even-odd nature of the IR intensities of the main active vibrational mode, odd-numbered cluster anions are predicted to cool faster. The experimentally scaled vibrational cooling rates of C_4^- and C_6^- obtained in the present study are shown in Fig. 8(b). Those of C_5^- and C_7^- are also shown with the the factors obtained previously [2,3,26]. As can be seen in Fig. 8(b), it is obvious that the even-odd alternation is absent. Simply stated, the larger the anion, the faster it cools. That is, the even-odd alternation in vibrational frequencies and IR intensities is not large enough to make a difference in the overall cooling rate of the hot anions.

IV. CONCLUSION

We measure the electronic and vibrational radiative cooling rate over a wide energy range from below to above the electronic excited states of C_4^- and C_6^-. Under both one- and two-photon absorption, the approach based on the energy window concept is a powerful tool to measure radiative cooling, especially for small ions, in which the window is fairly narrow. The present results show a significant reordering of the vibrational cooling rates as a function of size, relative to the theoretically predicted vibrational A coefficients. The method used is generally applicable and provides access to the complex process of vibrational radiative cooling, for which detailed theoretical predictions, to the best of our knowledge, do not exist.

ACKNOWLEDGMENTS

This work has been supported by JSPS Research Fellow and KAKENHI Grants No. JP16J04833, No. JP17H02937, and No. 26220607.

[1] H. T. Schmidt, Phys. Scr., T **166**, 014063 (2015).
[2] M. Goto, A. E. K. Sundén, H. Shiromaru, J. Matsumoto, H. Tanuma, T. Azuma, and K. Hansen, J. Chem. Phys. **139**, 054306 (2013).
[3] K. Najafian, M. S. Pettersson, B. Dynefors, H. Shiromaru, J. Matsumoto, H. Tanuma, T. Furukawa, T. Azuma, and K. Hansen, J. Chem. Phys. **140**, 104311 (2014).
[4] J. U. Andersen, P. Hvelplund, S. B. Nielsen, U. V. Pedersen, and S. Tomita, Phys. Rev. A **65**, 053202 (2002).
[5] S. Martin, J. Bernard, R. Brédy, B. Concina, C. Joblin, M. Ji, C. Ortega, and L. Chen, Phys. Rev. Lett. **110**, 063003 (2013).
[6] S. Martin, J. Matsumoto, N. Kono, M.-C. Ji, R. Brédy, J. Bernard, A. Cassimi, and L. Chen, Nucl. Instrum. Methods Phys. Res., Sect. B **408**, 209 (2017).
[7] P. Ferrari, J. Vanbuel, K. Hansen, P. Lievens, E. Janssens, and A. Fielicke, Phys. Rev. A **98**, 012501 (2018).
[8] P. Ferrari, E. Janssens, P. Lievens, and K. Hansen, J. Chem. Phys. **143**, 224313 (2015).
[9] M. Lange *et al.*, New J. Phys. **14**, 065007 (2012).

[10] G. Ito, T. Furukawa, H. Tanuma, J. Matsumoto, H. Shiromaru, T. Majima, M. Goto, T. Azuma, and K. Hansen, Phys. Rev. Lett. **112**, 183001 (2014).

[11] V. Chandrasekaran, B. Kafle, A. Prabhakaran, O. Heber, M. Rappaport, H. Rubinstein, D. Schwalm, Y. Toker, and D. Zajfman, J. Phys. Chem. Lett. **5**, 4078 (2014).

[12] N. Kono, T. Furukawa, H. Tanuma, J. Matsumoto, H. Shiromaru, T. Azuma, K. Najafian, M. S. Pettersson, B. Dynefors, and K. Hansen, Phys. Chem. Chem. Phys. **17**, 24732 (2015).

[13] Y. Ebara, T. Furukawa, J. Matsumoto, H. Tanuma, T. Azuma, H. Shiromaru, and K. Hansen, Phys. Rev. Lett. **117**, 133004 (2016).

[14] M. Yoshida, T. Furukawa, J. Matsumoto, H. Tanuma, T. Azuma, H. Shiromaru, and K. Hansen, J. Phys. Conf. Ser. **875**, 012017 (2017).

[15] D. W. Arnold, S. E. Bradforth, T. N. Kitsopoulos, and D. Neumark, J. Chem. Phys. **95**, 8753 (1991).

[16] P. Freivogel, M. Grutter, D. Forney, and J. P. Maier, J. Chem. Phys. **107**, 22 (1997).

[17] Y. Zhao, E. Beer, and D. M. Neumark, J. Chem. Phys. **105**, 2575 (1996).

[18] Z. Cao and S. D. Peyerimhoff, J. Phys. Chem. A **105**, 627 (2001).

[19] Y. Zhao, E. Beer, C. Xu, T. Taylor, and D. M. Neumark, J. Chem. Phys. **105**, 4905 (1996).

[20] V. Chandrasekaran, A. Prabhakaran, B. Kafle, H. Rubinstein, O. Heber, M. Rappaport, Y. Toker, and D. Zajfman, J. Chem. Phys. **146**, 094302 (2017).

[21] J. Szczepanski, S. Ekern, and M. Vala, J. Phys. Chem. A **101**, 1841 (1997).

[22] J. Szczepanski, E. Auerbach, and M. Vala, J. Phys. Chem. A **101**, 9296 (1997).

[23] S. Jinno, T. Takao, K. Hanada, M. Goto, K. Okuno, H. Tanuma, T. Azuma, and H. Shiromaru, Nucl. Instrum. Methods Phys. Res., Sect. A **572**, 568 (2007).

[24] T. Furukawa, G. Ito, M. Goto, T. Majima, H. Tanuma, J. Matsumoto, H. Shiromaru, K. Hansen, and T. Azuma, Nucl. Instrum. Methods Phys. Res., Sect. B **354**, 192 (2015).

[25] J. U. Andersen, E. Bonderup, and K. Hansen, J. Phys. B: At. Mol. Opt. Phys. **35**, R1 (2002).

[26] In Refs. [2], [3], and [24], the erroneous term of ln(10) is included, which is corrected in the present study.